



OPEN

PN/PAs-WSe₂ van der Waals heterostructures for solar cell and photodetector

Xinyi Zheng¹, Yadong Wei¹, Kaijuan Pang¹, Ngeywo Kaner Tolbert¹, Dalin Kong¹, Xiaodong Xu¹, Jianqun Yang², Xingji Li²✉ & Weiqi Li^{1,3}✉

By first-principles calculations, we investigate the geometric stability, electronic and optical properties of the type-II PN-WSe₂ and type-I PAs-WSe₂ van der Waals heterostructures (vdWH). They are *p*-type semiconductors with indirect band gaps of 1.09 eV and 1.08 eV based on PBE functional respectively. By applying the external gate field, the PAs-WSe₂ heterostructure would transform to the type-II band alignment from the type-I. With the increasing of magnitude of the electric field, two heterostructures turn into the *n*-type semiconductors and eventually into metal. Especially, PN/PAs-WSe₂ vdWH are both high refractive index materials at low frequencies and show negative refractive index at high frequencies. Because of the steady absorption in ultraviolet region, the PAs-WSe₂ heterostructure is a highly sensitive UV detector material with wide spectrum. The type-II PN-WSe₂ heterostructure possesses giant and broadband absorption in the near-infrared and visible regions, and its solar power conversion efficiency of 13.8% is higher than the reported GaTe-InSe (9.1%), MoS₂/p-Si (5.23%) and organic solar cells (11.7%). It does project PN-WSe₂ heterostructure a potential for application in excitons-based solar cells.

Since the first fabrication of monolayer graphene by mechanical stripping, two-dimensional (2D) materials have become the focus arising from their depicted excellent electronic and optical properties promising for a wide range of applications^{1,2}. Among emerging 2D materials family, black phosphorus (BP) exhibits other attractive properties, such as anisotropic optical properties and the highly tunable and thickness-dependent direct band gap. Despite its many great attractions, a major challenge to the application of BP for electronic and optical applications is its structural instability at ambient conditions. The presence of lone-pair electrons in phosphorene makes it reactive and it can easily absorb impurities with a strong binding energy resulting from the phosphorus to impurity charge transfer. Therefore, enhancing the stability of BP is critically important for device applications. More recently, It has been testified that the group-VA binary compounds 2D materials with the black phosphorene phase such as PN, PAs, AsN and AsSb etc. possess considerable and tunable band gaps, high charge carrier mobilities which exceed the transition metal dichalcogenides (TMDs) materials^{3,4}, leading to their favorable application in electronic and energy devices. The PN/PAs show the capability of high solar power conversion efficiency (PCE), pointing to the promising alternative materials for solar cells^{3,5,6}. Meanwhile, experimental studies have demonstrated that the PAs has utilization potentiality in the field of mid-infrared (MIR) photoelectron detectors⁵⁻⁷. The possibility of widening its electrical performance has also been revealed due to its fully tunable band gap^{8,9}. More importantly, group-VA binary compounds have shown good oxidation resist¹⁰. It has been demonstrated that combining the distinct 2D materials to construct heterostructures can engineer the electronic properties and bring new exciting physical phenomena. For example, the van der Waals heterostructures with type-II band alignment can substantially accelerate spatial separation of photogenerated electron-hole pairs to improve the efficiency of photoconversion. Moreover, it was found that a vertical electric field was able to tune the relative position of the band structure of component monolayers, which enables a controllable Schottky barrier height in the heterostructure. Thus, novel vdW heterostructures that consist of different 2D materials attracted extensive attention due to their unique electronic properties which have abundant opportunities for application in nano-optoelectronics^{11,12}.

In this paper, we extended properties of 2D monolayer materials, PN and PAs, by constructing vdW heterostructures with the monolayer WSe₂ which has great potential application in optoelectronic device due to its considerable and direct band gap and strong photoelectric response^{3,14}. Using first principle calculations, the

¹School of Physics, Harbin Institute of Technology, Harbin 150001, China. ²School of Materials Science and Engineering, Harbin Institute of Technology, Harbin 150001, China. ³Collaborative Innovation Center of Extreme Optics, Shanxi University, Taiyuan 030006, China. ✉email: lxj0218@hit.edu.cn; tccliweiqi@hit.edu.cn

PN-WSe₂ and PAs-WSe₂ vdW heterostructures were studied, focusing on their interesting electronic properties enabled by their gate-tunable band gaps and offsets. Their sensitive E-dependent band gaps and wide absorption spectrum offer a practical route to applications in optoelectronics and nano-electronics.

Calculation details

All calculations have been performed by using the Vienna ab initio simulation package (VASP)^{15–17}. Structure optimization have been performed based on the generalized gradient approximation (GGA) within Perdew–Burke–Ernzerhof (PBE) parameterization^{18,19}. The Monkhorst–Pack scheme with 9 × 9 × 1 k-point grid was used for the integration in the first Brillouin zone. The lattice parameters and ionic positions were fully relaxed until the total energies and forces were less than 10^{−5} eV and 0.01 eVÅ^{−1}, respectively. The DFT-D2 method of Grimme²⁰ was used to describe the weak dispersion forces. The vacuum space spanning was set to 40 Å in the z direction. For electronic structures calculation, a 13 × 13 × 1 Monkhorst–Pack mesh was used for both the DOS and band structure. Since PBE functional often underestimates the bandgaps, we have also calculated the band gaps at the HSE06²¹ level for comparison. Optical properties can be described by the dielectric function: $\varepsilon(\omega) = \varepsilon_1(\omega) + i\varepsilon_2(\omega)$, where $\varepsilon_1(\omega)$ is the real part and the $\varepsilon_2(\omega)$ is the imaginary part which also represents the dielectric loss. The imaginary part $\varepsilon_2(\omega)$ is obtained by calculating the band structure:

$$\varepsilon_{\alpha\beta}^{(2)}(\omega) = \frac{4\pi^2 e^2 \hbar^4}{\Omega \omega^2 m_e^4} \lim_{q \rightarrow 0} \sum_{cv} 2w_k \delta(\varepsilon_{ck+q} - \varepsilon_{vk} - \hbar\omega) \times u_{ck} |i\nabla_{\alpha} - k_{\alpha}| u_{ck} u_{ck} |i\nabla_{\beta} - k_{\beta}| u_{ck}$$

while the real part is obtained by through the Kramer–Kronig transformation:

$$\varepsilon_{\alpha\beta}^{(1)}(\omega) = 1 + \frac{2}{\pi} P \left[\int_0^{\infty} \frac{\varepsilon_{\alpha\beta}^{(2)}(\omega') \omega'}{\omega'^2 - \omega^2} d\omega' \right].$$

The absorption rate $\alpha(\omega)$ is

$$\alpha(\omega) = \sqrt{2}\omega \sqrt{\sqrt{\varepsilon_1^2(\omega) + \varepsilon_2^2(\omega)} - \varepsilon_1(\omega)}.$$

Results and discussion

Figure 1 demonstrates the fully optimized rectangular-cell structure of PN-WSe₂, PAs-WSe₂ vdW heterostructures and component monolayers with their corresponding band structure. The lattice constants of PN and PAs are a = 2.71 Å, b = 4.15 Å and a = 3.60 Å, b = 4.50 Å, respectively. The lattice constants of rectangular WSe₂ are a = 3.29 Å, b = 5.70 Å. The optimal interlayer distances of our heterostructures systems are 3.02 Å (PN-WSe₂) and 3.12 Å (PAs-WSe₂) through the minimum total energy calculation. These values are smaller than the results of 3.17 Å reported for bP-MoSSe vdW heterostructure²². The stability of the two heterostructures determined by the binding energy E_b . The formula of the binding energy is:

$$E_b = (E - E_1 - E_2)/N$$

where E is the total energy of the heterostructure, E_1 is the energy of the isolated PN/PAs monolayer, E_2 is the isolated WSe₂ monolayer's energy and N is the total number of atoms in the heterostructure. For the stable stack modes with minimum stress presented in Fig. 1b,c, the average stress of both materials is 0.97% (PN-WSe₂) and 0.82% (PAs-WSe₂). And the binding energies for PN-WSe₂ and PAs-WSe₂ are −320 meV and −250 meV, respectively. These values are relatively lower than other possible modes as shown in Table S1 and Table.S2, indicating that WSe₂ monolayer can combine with the PAs or PN monolayers to form a stable vdWH. As we have known that the band gaps of all structures in GGA-PBE level are lower than HSE06 results. PBE functional predicted that PN monolayer is semiconducting with indirect band gap (Γ-X) of 1.66 eV, whereas PAs monolayer has a direct band gap of 0.87 eV at Γ point. The WSe₂ monolayer shows a direct band gap of 1.67 eV. Based on HSE06 hybrid functional, band gaps of PN, PAs and WSe₂ monolayers are 2.72, 1.29 and 2.16 eV respectively. As shown in Fig. 2, the work functions of PN, PAs and WSe₂ monolayers are 5.14, 4.39 and 4.54 eV on the PBE level. Because their VBM are much closer to the Fermi Level than the CBM, the PN-WSe₂ and PAs-WSe₂ heterostructures are both *p*-type semiconductors with 1.09 and 1.08 eV band gaps from the Fig. 3. The similar character is also predicted by using HSE06 hybrid functional. The HSE06 band gaps of PN-WSe₂ and PAs-WSe₂ heterostructures are 1.88 and 1.75 eV. The values of work function of PN, PAs and WSe₂ monolayers are 5.89, 4.92 and 5.12 eV as shown in supplementary information, respectively. In theoretical levels based on PBE and HSE06, the CBM of PAs is lower than that of WSe₂, whereas its VBM is higher than that of WSe₂. It indicates that the PAs-WSe₂ heterostructure is a type-I band alignment heterostructure, while for the PN-WSe₂ heterostructure, the CBM of PN is lower than that of WSe₂, whereas the VBM of WSe₂ is higher than that of PN, indicating that the PN-WSe₂ heterostructure has a typical type-II band alignment structure.

Figure 3a,b show the projected band structures of two heterostructures based on PBE calculation, respectively. For the PN-WSe₂ vdW heterostructure, its CBM is contributed by PN monolayer while the VBM is contributed by WSe₂ monolayer which shows the typical characteristic of type-II band alignment in Fig. 2. It involuntarily separates the electron and hole distributions. Moreover, with projected density of states of vdW heterostructures shown in Fig. 3c,d, it can be seen that the W and Se elements, especially d orbitals of W which is displayed on Fig. 3e,f, have great contribution to the density of states of two heterostructures near the Fermi level. For PAs-WSe₂ band structure, the type-I band alignment could be testified by its only one band edge contributor PAs

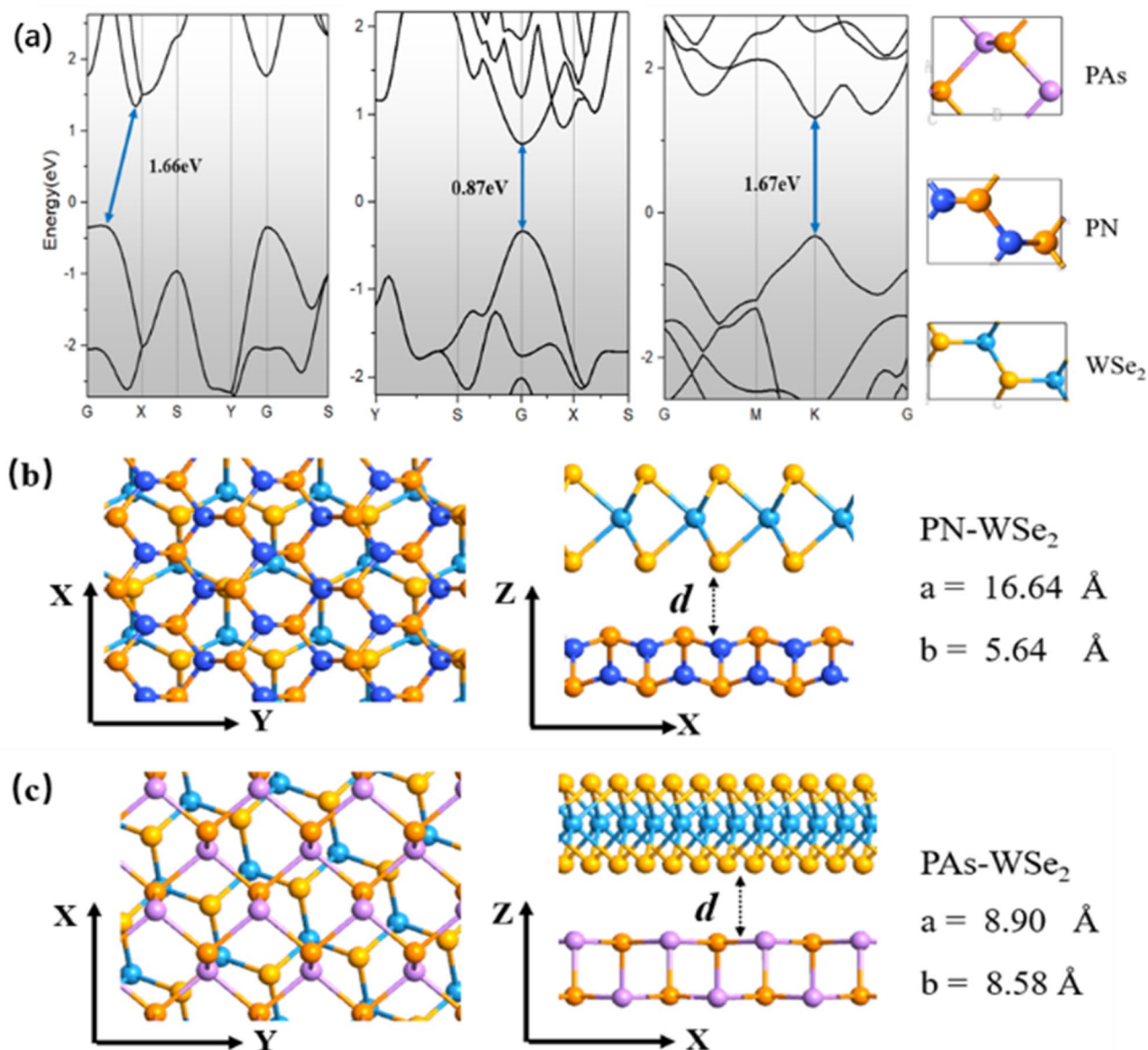


Figure 1. (a) The band structures and single optimized rectangular-cell structures of PN, PAs and WSe₂ are shown; (b) The top view, side view and lattice constants of PN-WSe₂ vdW heterostructure are presented. Deep blue is N, light blue is W, yellow is Se and orange is P. Where the d , the a and the b represent the distance between two monolayers in the heterostructure and lattice constants, respectively; (c) The top view, side view and lattice constants of PAs-WSe₂ vdW heterostructure are presented. Purple is As, light blue is W, yellow is Se and orange is P.

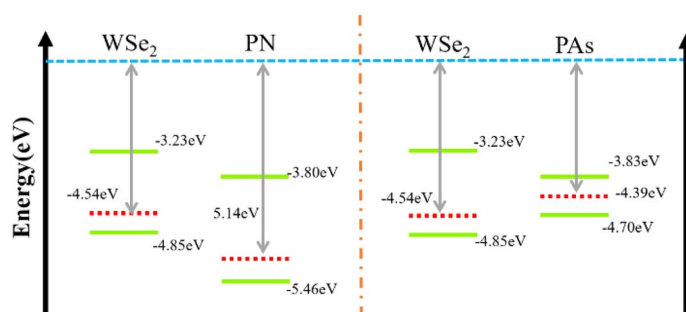


Figure 2. The work function and the position of CBM and VBM relative to the vacuum energy level of WSe₂, PN, PAs in PBE theoretical level.

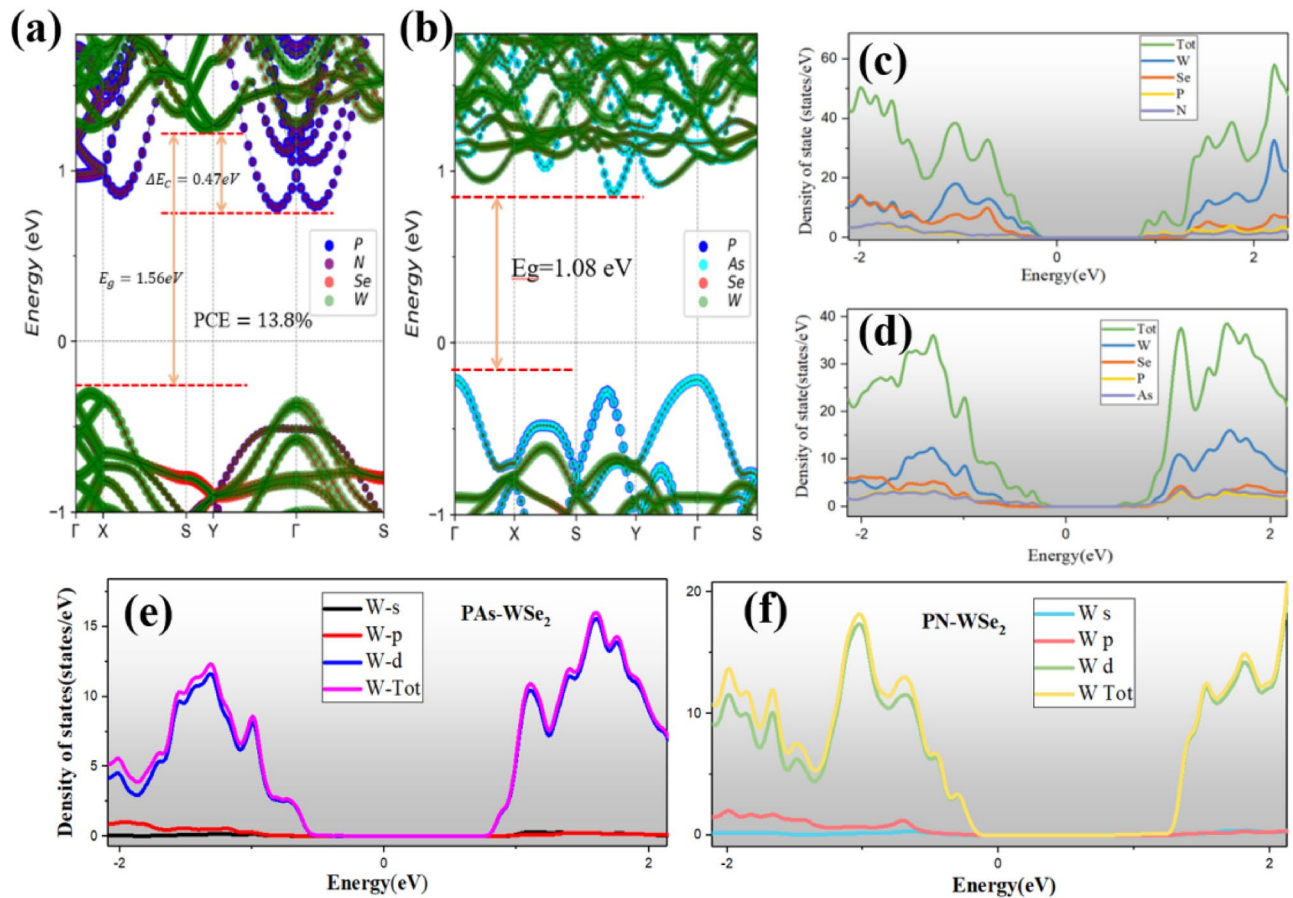


Figure 3. (a,b) The band structure for PN-WSe₂ and PAs-WSe₂ vdW heterostructure; (c,d) The total and projected DOS of PN-WSe₂ and PAs-WSe₂ vdW heterostructure; (e,f) The contribution from W-orbitals for DOS of PAs-WSe₂ and PN-WSe₂ vdW heterostructure;

which also could be shown in Fig. 2. Despite of some discrepancy in the bandgaps of heterostructures, PBE and HSE06 functionals provide the same band structure and band alignment type. Thus, we only utilize PBE level band structure in following discussion.

In some experiments, the electrostatic gating is an effective way to modulate the electronic characteristics of the vdW heterostructure. By applying the electrical field perpendicular to 2D layers (along z -direction) in the range ± 0.25 V/Å, two heterostructures show modulation of band gap. Figure 4a,b demonstrate the fitting curve of the band gap under the electrical field (the correlation coefficients are 0.9834 and 0.9562, respectively). It should be pointed out that variation of band gap shows asymmetric behavior under two opposite electric fields. e.g. The positive field reduces band gap of the PAs-WSe₂ vdW heterostructure sharply and leads to a transition from semiconductor to metal at $E = 0.22$ V/Å. The negative field firstly increases the band gap to a maximum value 1.19 eV at $E = -0.025$ V/Å and then decreases continuously to minimum 0 eV. On the contrary, for the PN-WSe₂ vdW heterostructure, it is the negative field that reduces the band gap to 0 eV at $E = -0.20$ V/Å, while the positive field make the band gap to a maximum value 1.52 eV at $E = 0.075$ V/Å and then decreases to 0 eV. It indicated that they possess an inherent electric dipole moment with magnitude 0.075 V/Å and 0.025 V/Å respectively, whose direction depends on materials internal electrostatic potential. Surprisingly, magnitude of electric field causing phase transition of PN/PAs-WSe₂ heterostructures are much smaller than recently reported BP-MoSe₂ vdW heterostructure of 1 V/Å²³ and BP-MoSSe vdW heterostructure of 0.8 V/Å²². The projected band structures of the PN-WSe₂ vdW heterostructures with different electrical field are presented from Fig. 4c–g, while the effect on the band structure of PAs-WSe₂ vdW heterostructures are shown in Fig. 4h–l. For the PN-WSe₂ vdW heterostructure, when the external electrical field increases along the positive direction, in contrast to free heterostructure, the PN monolayer has larger contribution to the CBM whereas contribution of WSe₂ in VBM increases with the band edge position approaching each other as shown in Fig. 4e–g. For the PAs-WSe₂ vdW heterostructure, when the electrical field along the positive direction increases, contributions of PAs to the CBM increase whereas leading to more contributions from WSe₂ to the VBM as shown in Fig. 4j–l. Under the negative electric field, we can see the different effect as shown in Fig. 4h,i. When the magnitude of the applied electric field reaches 0.1 V/Å, WSe₂ has large contribution to both VBM and CBM. It suggests that the PAs-WSe₂ heterostructure will transform from type-I to type-II band alignment by the electric field which could be used in high-performance optoelectronic nanodevices. In addition, we found the PN-WSe₂ vdW heterostructure would transform to n -type semiconductor from p -type semiconductor if the external electric field is large enough

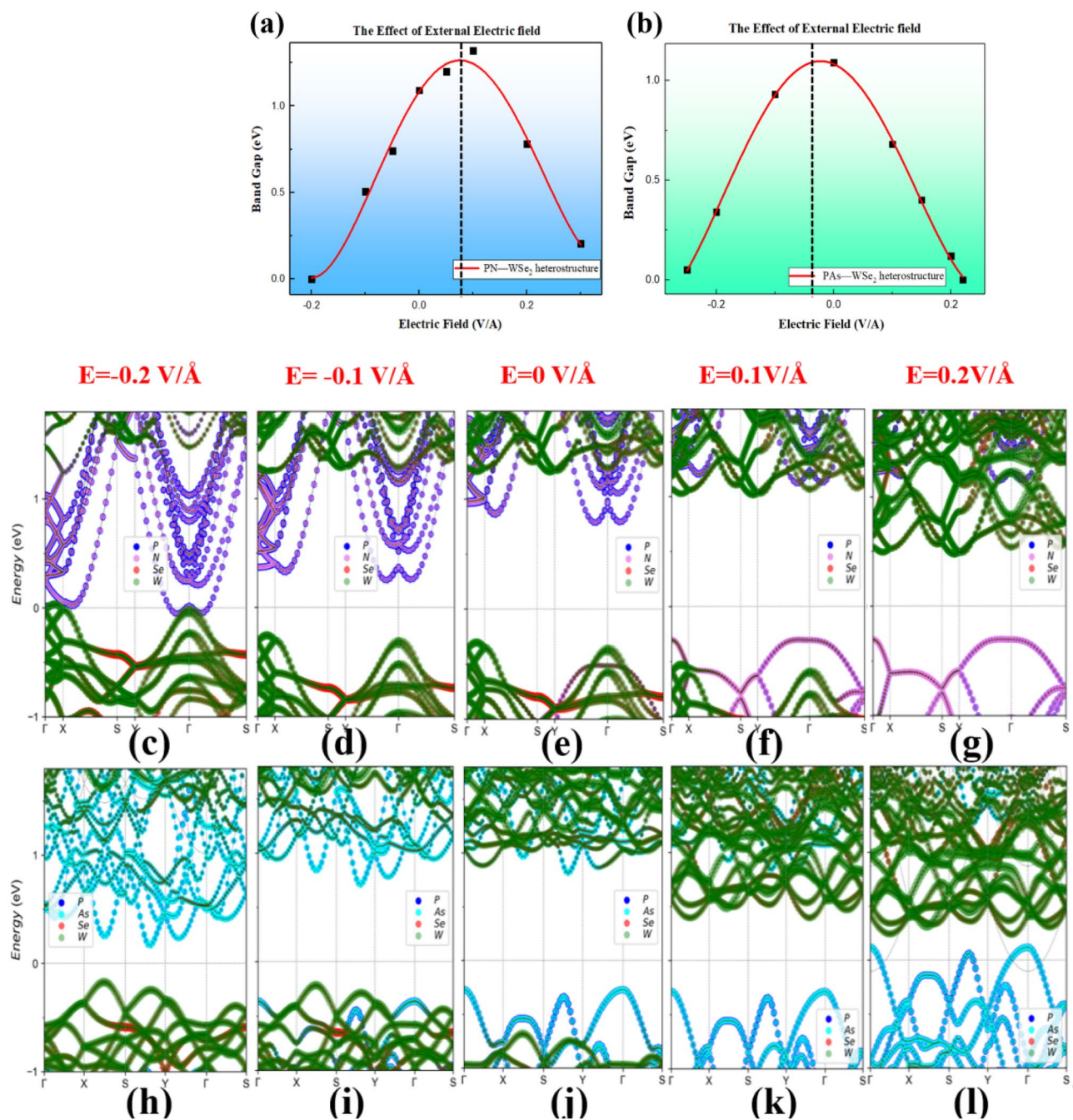


Figure 4. (a,b) The bandgap modulation by external electrical field, and the band structure under the effect of external electrical field ((c–g): PN-WSe₂, (h–l): PAs-WSe₂).

regardless of direction. However for the PAs-WSe₂ vdW heterostructure, only increasing the electrical field in negative direction could induce a transition from *p*-type semiconductor to *n*-type semiconductor. The asymmetric behavior of the band gap modulated by the electrical field can be attributed to the balance between the external electrical field and the internal electrical field of the heterostructures, which are caused by the uneven distribution of charge densities inside the heterostructures when two different components are stacked together by van der Waals interaction²⁴.

Many-body effect has a profound impact on the optical properties of 2D materials due to reduced coulomb screening. The Bethe–Salpeter approach can achieve a convincing agreement with experimental absorption spectra. In this work, instead, we introduce the so called scissors correction (SCI) to reduce the errors caused by the neglected many-body effects. The imaginary part of dielectric function of the PN/PAs-WSe₂ vdW heterostructure along the *y*-direction are shown in Fig. S1 and Fig. S2. It indicates that the heterostructures have obvious exciton effect. However, our calculated results show that the shape of the spectrum based on IPA + scissors correction can reproduce that of GW + BSE. Considering the high computational cost of BSE, and also for comparison with the results reported PCE of other 2D heterostructures, the linear optical properties are discussed on basis of the

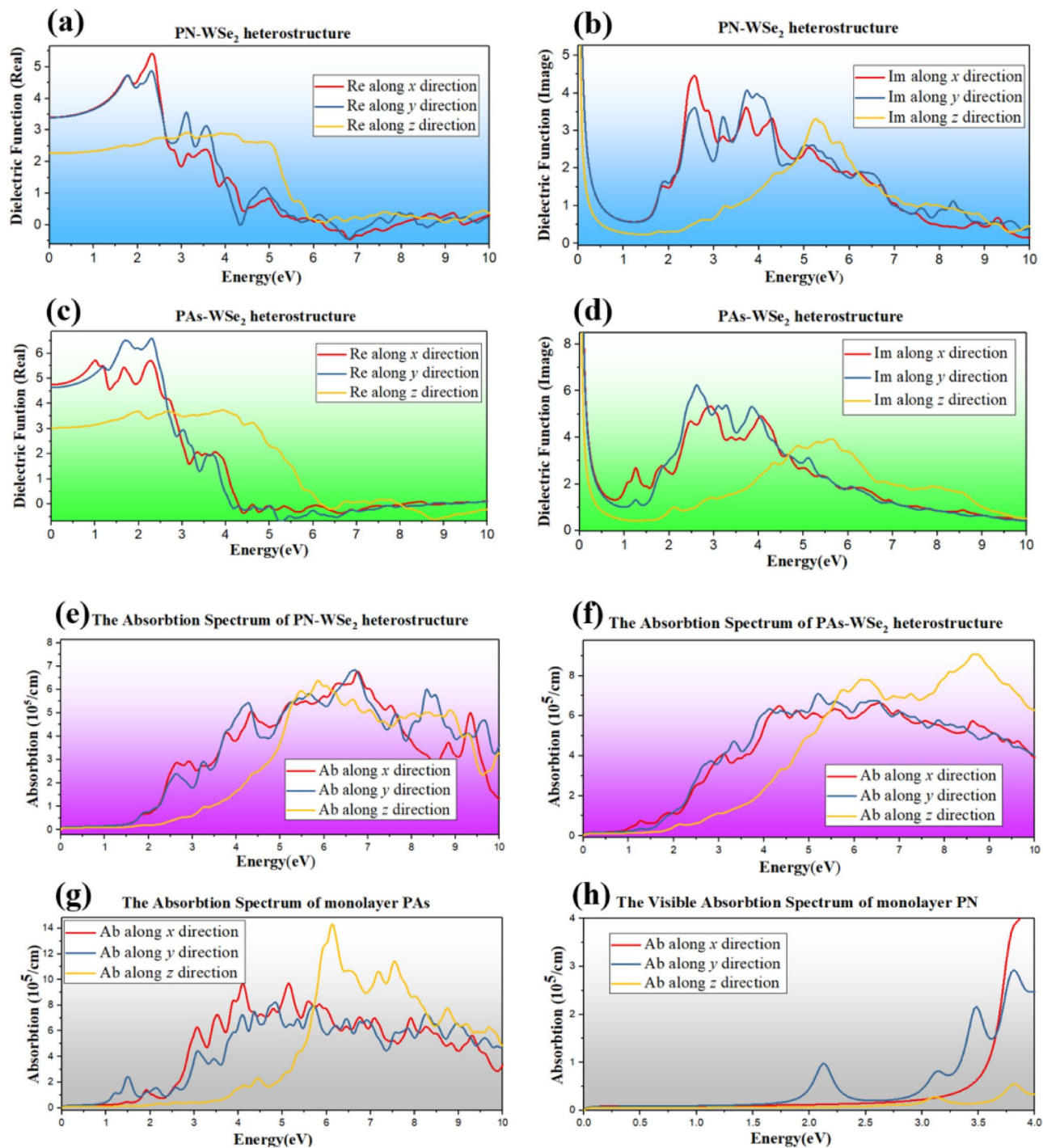


Figure 5. (a,b) The dielectric function's real and imaginary part of PN-WSe₂ vdW heterostructure; (c,d) The dielectric function's real and imaginary part of PAs-WSe₂ heterostructure in 0–10 eV; (e,f) The absorption spectrum of PN/PAs-WSe₂ heterostructure in 0–10 eV; (g) The absorption spectrum of monolayer PN in visible light region; (h) The absorption spectrum of monolayer PAs in 0–10 eV.

independent-particle approximation (IPA) with scissors correction in present work. As shown in the Fig. 5a,c, the PN/PAs-WSe₂ vdW heterostructures have the dielectric characteristic with high refractive index at low frequencies and the metallic character due to negative refractive index at high frequencies. In particular, the dielectric functions for linear polarization along x and y direction can reach 5.42 and 6.58 at 2.33 eV, respectively. Although the dielectric functions along vertical polarization (z) are smaller than that along horizontal polarization (x and y), they also show strong response in the visible light region (0–5 eV). For the imaginary part, in case of horizontal polarization, PAs-WSe₂ vdW heterostructures have three peaks at 2.57, 3.73 and 5.25 eV. There are three major peaks in 2.92, 2.62 and 5.65 eV for PN-WSe₂ vdW heterostructure, which are shown in Fig. 5b,d. For the PN-WSe₂ vdW heterostructures, there is a strong and wide absorption peak in visible region

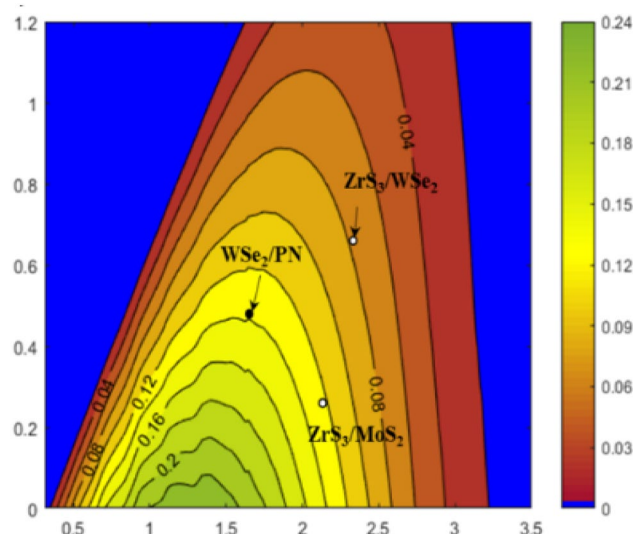


Figure 6. Power Conversion Efficiency contour computed plot. The black solid point marks the position of the type-II PN-WSe₂ vdW heterostructure. The white hole shows the PCE for two novel heterostructures of ZrS₃-MoS₂ and ZrS₃-WSe₂²⁸.

(350–682 nm) compared with component PN monolayer, especially for the z-direction components as shown in Fig. 5e, the absorption intensity of heterostructure is 30 times higher than that of PN monolayer in Fig. 5h. It could be interpreted that strong interlayer coupling leads to denser DOS for those heterostructures. It is clearly that the type II band structure of PN-WSe₂ vdW heterostructure and large absorption coefficient in visible light region ensure its potential application for solar cells which be estimated quantitatively by the power conversion efficiency (PCE) formula given by Scharber et al.²⁵ The upper limit for PCE can be described as:

$$\eta = \frac{J_{sc} V_{oc} \beta_{FF}}{P_{solar}} = \frac{0.65 \left(E_g^d - \Delta E_c - 0.3 \right) \int_{E_g^d}^{\infty} \frac{J_{ph}(\hbar\omega)}{\hbar\omega} d(\hbar\omega)}{\int_0^{\infty} J_{ph}(\hbar\omega) d(\hbar\omega)}$$

From the band alignment in Fig. 3a, the band gap of WSe₂ donor is $E_g^d = 1.56$ eV, the conduction band offset (CBO) for PN-WSe₂ vdW heterostructure is $\Delta E_c = 0.47$ eV, the band fill factor β_{FF} is 0.65 and the 0.3 eV is the empirical estimation of kinetic energy conversion loss²⁵. $J_{ph}(\hbar\omega)$ is AM1.5 solar energy flux ($\text{Wm}^{-2} \text{eV}^{-1}$). As shown in Fig. 6, the solar power conversion efficiency contour at efficiency of 13.8%, PN-WSe₂ vdW heterostructure possesses a high PCE at the level of CBO, higher than the organic solar cells (11.7%)²⁶ vdW heterostructure, the MoS₂/p-Si solar cells (5.23%)²⁷ vdW heterostructure and the type-II GaTe-InSe (9.1%)²⁸ which are recently reported. This is attributed to the reduced band gap of PN donor in contrast to that of MoS₂ and reduced CBM differences between PN and WSe₂ monolayers. The result illustrates a new approach for an efficient solar energy conversion on PN-WSe₂ vdW heterostructure in 2D excitonic solar cells.

For PAs-WSe₂ vdW heterostructure in Fig. 5f, it has a very strong absorption peak is at 8.62 eV with absorption coefficient $9.1 \times 10^5/\text{cm}$ and extremely wide absorption band in the ultraviolet region when it is polarized along vertical direction. Compared with the Janus b-PAs²⁹, α -PAs has a larger direct optical band gap and relative high response at the peak area because of the different crystal structure. But when introducing it into heterostructure with WSe₂, as shown in Fig. 5g, the high response occurs blue shift and shows high absorption characteristics in the ultraviolet region, which is more wide and gentle change before 10 eV. It implies that PAs-WSe₂ vdW heterostructure is the potential candidate for highly sensitive UV detectors.

Summary

In summary, we have systematically predicted the electronic and optical properties of PN/PAs (Black Phosphorus phase)-WSe₂ vdW heterostructures with indirect and tunable band gaps and their modulations under the external electrical field. For the PAs-WSe₂ vdW heterostructure, its VBM and CBM are both contributed by PAs monolayer, resulting in type-I band alignment. Whereas for the PN-WSe₂ vdW heterostructure, its VBM and CBM results from WSe₂ and PN monolayer respectively, which leads to a type-II band alignment indicating it is beneficial to the spatial separation of photogenerated electron–hole pairs. The external electrical field not only tunes both heterostructures' band edges, contributors of VBM and CBM and band gaps, but also changes the Schottky barrier from *p*-type to *n*-type and turns the PAs-WSe₂ vdW heterostructure into a type-II heterostructure from type-I. Furthermore, this research also predicts they have strong and considerable highly anisotropic optical response, which greatly enhance the optical performance of PN and PAs, enabling novel applications in optoelectronics from visible to ultraviolet regions. The extremely wide absorption spectrum in the ultraviolet

region makes the PAs-WSe₂ heterostructure is likely to become an alternative UV detector material. For the type-II PN-WSe₂ heterostructure, it has a great visible light absorption and the high solar PCE at the level of CBO of 13.8%. It does show great application potential in exciton solar cells. Our results demonstrate that these two 2D-materials have great potential in the application of nano-optoelectronic devices based on van der Waals heterostructure.

Data availability

The data that supports the findings are available upon request from the corresponding author.

Received: 22 May 2020; Accepted: 3 September 2020

Published online: 14 October 2020

References

- Xu, K. *et al.* The role of Anderson's rule in determining electronic, optical and transport properties of transition metal dichalcogenide heterostructures. *Phys. Chem. Chem. Phys.* **20**, 30351–30364. <https://doi.org/10.1039/c8cp05522j> (2018).
- Hu, X. R., Zheng, J. M. & Ren, Z. Y. Strong interlayer coupling in phosphorene/graphene van der Waals heterostructure: a first-principles investigation. *Front Phys-Beijing* <https://doi.org/10.1007/s11467-017-0736-0> (2018).
- Guo, S. Y. *et al.* 2D V-V binary materials: status and challenges. *Adv. Mater* **31**, e1902352. <https://doi.org/10.1002/adma.201902352> (2019).
- Zhang, S. L. *et al.* Recent progress in 2D group-VA semiconductors: from theory to experiment. *Chem. Soc. Rev.* **47**, 982–1021. <https://doi.org/10.1039/c7cs00125h> (2018).
- Amani, M., Regan, E., Bullock, J., Ahn, G. H. & Javey, A. Mid-wave infrared photoconductors based on black phosphorus-arsenic alloys. *ACS Nano* **11**, 11724–11731. <https://doi.org/10.1021/acsnano.7b07028> (2017).
- Xiao, W. Z., Xiao, G., Rong, Q. Y. & Wang, L. L. Theoretical discovery of novel two-dimensional V-A-N binary compounds with auxiticity. *Phys. Chem. Chem. Phys.* **20**, 22027–22037. <https://doi.org/10.1039/c8cp04158j> (2018).
- Long, M. S., Gao, A. Y. & Wang, P. Room temperature high-detectivity mid-infrared photodetectors based on black arsenic phosphorus. *Sci. Adv.* **3**, e1700589. <https://doi.org/10.1126/sciadv.1700589> (2017).
- Sun, Y. J., Shuai, Z. G. & Wang, D. Lattice thermal conductivity of monolayer AsP from first-principles molecular dynamics. *Phys. Chem. Chem. Phys.* **20**, 14024–14030. <https://doi.org/10.1039/c8cp01840e> (2018).
- Khang, N. H. D., Ueda, Y. & Hai, P. N. A conductive topological insulator with large spin Hall effect for ultralow power spin-orbit torque switching. *Nat. Mater.* <https://doi.org/10.1038/s41563-018-0137-y> (2018).
- Wei, Y. D. *et al.* Long radiation lifetime and quasi-isotropic excitons in antioxidant V–V binary phosphorene allotropes with intrinsic dipole. *J. Phys. Chem. C* <https://doi.org/10.1021/acs.jpcc.0c03156> (2020).
- Zhang, W. & Zhang, L. F. Electric field tunable band-gap crossover in black(blue) phosphorus/g-ZnO van der Waals heterostructures. *RSC Adv.* **7**, 34584–34590. <https://doi.org/10.1039/c7ra06097a> (2017).
- Srivastava, P. K., Hassan, Y. & Gebredingle, Y. Van der Waals Broken-Gap p-n heterojunction tunnel diode based on black phosphorus and rhenium disulfide. *ACS Appl. Mater. Inter.* **11**, 8266–8275. <https://doi.org/10.1021/acami.8b22103> (2019).
- Xia, C., Du, J., Li, M., Li, X. & Li, J. Effects of electric field on the electronic structures of broken-gap phosphorene/SnX₂ (X = S, Se) van der Waals heterojunctions. *Phys. Rev. Appl.* <https://doi.org/10.1103/PhysRevApplied.10.054064> (2018).
- Roy, T. *et al.* 2D–2D tunneling field-effect transistors using WSe₂/SnSe₂ heterostructures. *Appl. Phys. Lett.* **108**, 083111. <https://doi.org/10.1063/1.4942647> (2016).
- Kresse, G. Ab-initio molecular-dynamics for liquid-metals. *J. Non-Cryst Solids* **193**, 222–229. [https://doi.org/10.1016/0022-3093\(95\)00355-X](https://doi.org/10.1016/0022-3093(95)00355-X) (1995).
- Kresse, G. & Furthmüller, J. Efficiency of ab-initio total energy calculations for metals and semiconductors using a plane-wave basis set. *Comput. Mater. Sci.* **6**, 15–50. [https://doi.org/10.1016/0927-0256\(96\)00008-0](https://doi.org/10.1016/0927-0256(96)00008-0) (1996).
- Kresse, G. & Furthmüller, J. Efficient iterative schemes for ab initio total-energy calculations using a plane-wave basis set. *Phys. Rev. B* **54**, 11169–11186. <https://doi.org/10.1103/PhysRevB.54.11169> (1996).
- Perdew, J. P., Burke, K. & Ernzerhof, M. Generalized gradient approximation made simple. *Phys. Rev. Lett.* **77**, 3865–3868. <https://doi.org/10.1103/PhysRevLett.77.3865> (1996).
- Perdew, J. P., Burke, K. & Ernzerhof, M. Generalized gradient approximation made simple (vol 77, pg 3865, 1996). *Phys. Rev. Lett.* **78**, 1396–1396. <https://doi.org/10.1103/PhysRevLett.78.1396> (1997).
- Grimme, S. Accurate description of van der Waals complexes by density functional theory including empirical corrections. *J. Comput. Chem.* **25**, 1463–1473. <https://doi.org/10.1002/jcc.20078> (2004).
- Krukau, A. V., Vydrov, O. A., Izmaylov, A. F. & Scuseria, G. E. Influence of the exchange screening parameter on the performance of screened hybrid functionals. *J. Chem. Phys.* **125**, 224106. <https://doi.org/10.1063/1.2204597> (2006).
- Chen, D. C. *et al.* Tunable electronic structures in BP/MoSSe van der Waals heterostructures by external electric field and strain. *Appl. Surf. Sci.* **497**, 143809. <https://doi.org/10.1016/j.apsusc.2019.143809> (2019).
- Kaur, S., Kumar, A., Srivastava, S. & Tankeshwar, K. Van der Waals heterostructures based on allotropes of phosphorene and MoSe₂. *Phys. Chem. Chem. Phys.* **19**, 22023–22032. <https://doi.org/10.1039/c7cp03960c> (2017).
- Li, H. L., Cui, Y. T., Li, D. M. & Luo, H. J. Tuning the band alignment of p-type graphene-AsSb Schottky contact by electric field. *J. Appl. Phys.* **124**, 204301. <https://doi.org/10.1063/1.5054614> (2018).
- Scharber, M. C. *et al.* Design rules for donors in bulk-heterojunction solar cells: towards 10 % energy-conversion efficiency. *Adv. Mater* **18**, 789. <https://doi.org/10.1002/adma.200501717> (2006).
- Zhao, J. *et al.* Efficient organic solar cells processed from hydrocarbon solvents. *Nat. Energy* <https://doi.org/10.1038/Nenergy.2015.27> (2016).
- Tsai, M. L. *et al.* Monolayer MoS₂ heterojunction solar cells. *ACS Nano* **8**, 8317–8322. <https://doi.org/10.1021/nn502776h> (2014).
- Rawat, A., Dimple, R. A., Jena, N., Mohanta, M. K. & De Sarkar, A. Solar energy harvesting in type II van der Waals heterostructures of semiconducting group III monochalcogenide monolayers. *J. Phys. Chem. C* **123**, 12666–12675. <https://doi.org/10.1021/acs.jpcc.9b03359> (2019).
- Li, L. L. *et al.* Single-layer Janus black arsenic-phosphorus (b-AsP): optical dichroism, anisotropic vibrational, thermal, and elastic properties. *Phys. Rev. B* **101**, 134102. <https://doi.org/10.1103/PhysRevB.101.134102> (2020).

Acknowledgements

This work is supported by National Natural Science Foundation of China (Grant Nos. 11974091, 21673025).

Author contributions

X.Z. and Y.W. performed calculations and wrote main text of the manuscript. D.K. and W.L. performed figure generation and statistical analysis. K.P. and X.X. provided useful information for the power conversion efficiency. N.T.K., J.Y. and X.L. checked the spelling and grammar in the manuscript. All authors reviewed the manuscript.

Competing interests

The authors declare no competing interests.

Additional information

Supplementary information is available for this paper at <https://doi.org/10.1038/s41598-020-73152-7>.

Correspondence and requests for materials should be addressed to X.L. or W.L.

Reprints and permissions information is available at www.nature.com/reprints.

Publisher's note Springer Nature remains neutral with regard to jurisdictional claims in published maps and institutional affiliations.



Open Access This article is licensed under a Creative Commons Attribution 4.0 International License, which permits use, sharing, adaptation, distribution and reproduction in any medium or format, as long as you give appropriate credit to the original author(s) and the source, provide a link to the Creative Commons licence, and indicate if changes were made. The images or other third party material in this article are included in the article's Creative Commons licence, unless indicated otherwise in a credit line to the material. If material is not included in the article's Creative Commons licence and your intended use is not permitted by statutory regulation or exceeds the permitted use, you will need to obtain permission directly from the copyright holder. To view a copy of this licence, visit <http://creativecommons.org/licenses/by/4.0/>.

© The Author(s) 2020